crystals

MDPI

Article

Influence of the Substrate on the Exchange Coupling of NiO/FeCo Bilayers

Iker Lorenzo-Feijoo [1,2], Aida Serrano [3], Cayetano Hernández-Gómez [1], José Luis F. Cuñado [4,5] and Pilar Prieto [1,5,*]

1 Departamento de Física Aplicada, M-12 Universidad Autónoma de Madrid, 28049 Madrid, Spain; iker.lorenzo@estudiante.uam.es (I.L.-F.); cayetano.hernandez@estudiante.uam.es (C.H.-G.)
2 Departamento de Física de Materiales, Universidad Complutense, 28040 Madrid, Spain
3 Departamento de Electrocerámica, Instituto de Cerámica y Vidrio (ICV), Consejo Superior de Investigaciones Científicas, 28049 Madrid, Spain; aida.serrano@icv.csic.es
4 IMDEA Nanociencia, Faraday 9, 28049 Madrid, Spain; joseluis.fcunnado@imdea.org
5 Instituto Nicolás Cabrera (INC), Universidad Autónoma de Madrid, 28049 Madrid, Spain
* Correspondence: pilar.prieto@uam.es

Abstract: Antiferromagnetic/ferromagnetic (AF/F) systems have been extensively investigated due to the importance that interfacial exchange coupling effects have in the development of magnetic storage technologies. Recently, these systems have garnered interest for the potential they have to imprint the magnetic moments of the AF into an F layer, offering the possibility of using it as a read-out mechanism in antiferromagnetic spintronics. In this study, we explored the importance of crystalline orientation and strains induced by the substrate in the exchange coupling properties of NiO/FeCo AF/F bilayers. For that, we have grown NiO/FeCo bilayers on MgO (001) and Al_2O_3 (0001) substrates varying the FeCo layer thickness. In addition, we have analyzed both deposited samples and those with induced interfacial unidirectional anisotropy. For inducing such interfacial anisotropy, we used a field cooling procedure, heating the bilayers to 650 K and subsequently cooling down to room temperature under the presence of an external magnetic field of 300 mT. We have investigated the effect of the substrate in terms of crystalline orientation and lattice mismatching on the AF/F exchange coupling as well as the dependence of the coercivity and exchange bias on the inverse F layer thickness that is consistent with the interfacial origin of the AF/F exchange coupling. Moreover, the angular dependence of the magnetic properties was explored by using vectorial Kerr magnetometry, confirming the presence of both magnetocrystalline anisotropy, arising from the epitaxial character of the growing process mainly when the bilayer is grown on MgO (001) substrates, and the field cooling (FC)-induced unidirectional anisotropy.

Keywords: antiferromagnetic; exchange-coupling; NiO; epitaxial films

Citation: Lorenzo-Feijoo, I.; Serrano, A.; Hernández-Gómez, C.; F. Cuñado, J.L.; Prieto, P. Influence of the Substrate on the Exchange Coupling of NiO/FeCo Bilayers. *Crystals* **2024**, *14*, 369. https://doi.org/10.3390/cryst14040369

Academic Editor: John A. Mydosh

Received: 21 March 2024
Revised: 9 April 2024
Accepted: 11 April 2024
Published: 16 April 2024

1. Introduction

Antiferromagnetic materials (AFMs) have recently attracted attention due to their potential application as the active element for spintronic applications [1,2], hence being a potential substitute for ferromagnetic materials (FMs) in the next generation of spintronic devices due to their potentially unmatched characteristics. AFMs present two or more ordered but opposed magnetic sublattices, resulting in zero net magnetization. This makes them insensitive to external magnetic fields, allowing them to exhibit domains with different spin orders that are robust against external magnetic perturbations. They can achieve high-frequency spin transport dynamics with speeds reaching the THz domain [3]. Combined with their ultra-low Gilbert damping [4], the absence of stray fields, and good spin current conduction [5], they have become very promising materials for ultra-high-density magnetic storage technologies or ultrafast switching applications.

Antiferromagnetic/ferromagnetic (AF/F) bilayers have attracted special interest in the last decades due to their impact on spintronic applications. The exchange coupling effects at the interface between an antiferromagnet and a ferromagnet [6,7] are currently exploited in ferromagnetic spin valves. These devices comprise a pair of fixed and free ferromagnetic layers and they are the basis of commercial magnetic field sensors and magnetic random-access memories (MRAMs) [8]. In this arrangement, the antiferromagnetic moments are assumed to be fixed, and the antiferromagnet plays only a passive supporting role in the spintronic device. Through exchange coupling, the antiferromagnet enhances the magnetic hardness of the fixed reference layer. Another recent approach to AF/F systems occurs when a thin FM is coupled to a much thicker epitaxial AFM to operate as a readout mechanism for antiferromagnetic spintronic [9].

Apart from artificial antiferromagnets, nickel oxide (NiO) is one of the AFMs that are attracting recent interest for room-temperature applications, for example, in spintronic-based broadband THz emission [10]. NiO is an exemplary Mott insulator with a cubic rock-salt-phase structure above the Néel temperature (T_N = 523 K) that has a very complex domain structure including twin and spin domains and double domain walls, whose sizes depend on deposition conditions [11,12]. The atomic planes of Ni^{2+} ions with opposite spins are arranged in alternating order along the (111) direction, and this can introduce a slight rhombohedral distortion in the crystal structure [13].

NiO thin films can be grown epitaxially on oxide single-crystal substrates. The common rock-salt structure with a similar lattice constant of MgO and NiO (i.e., lattice mismatch < 1%) turns MgO into an ideal substrate for cube-on-cube epitaxial growth [14]. NiO (111) thin films can be grown on Al_2O_3 (0001) substrates, in which a biepitaxial growth with two types of domains rotated 60° has been observed [15,16]. The crystalline orientation and the strain induced by the epitaxial growth on both kinds of substrate are important to determine the AF character of NiO. The importance of NiO crystal orientation on the efficiency of generating THz spin-currents in the NiO/Pt system was recently demonstrated, resulting in a dependence on the orientation and thickness of the AF films [10].

In this work, we focus our study on the effects induced by the substrate on the exchange coupling properties of epitaxial NiO/FeCo bilayers deposited on both MgO (001) and Al_2O_3 (0001) substrates. Among the 3d ferromagnets with a BCC structure, FeCo was chosen as the F layer because of its soft magnetic behavior with the highest magnetic moment [17]. Most of the works on metallic NiO/F hybrid systems are concentrated on Fe and permalloy [18–20] as the F layer. NiO/Fe is studied as a model system since Fe can grow epitaxially on NiO (001) and most of the works are focused on the NiO/Fe interface [18,19]. In this case, the AF spins are rotatable following the orientation of the Fe spins [19]. In the case of NiO/$Fe_{20}Ni_{80}$, dynamic properties and the effects on non-collinear anisotropies induced in the system have been studied, mainly in polycrystalline layers [20]. However, exchange coupling studies on NiO/FeCo heterostructures are scarce [21]. The use of FeCo as an F layer in the exchange-coupled AF/F systems could offer some advantages for exchange-coupled-based devices related to its high magnetic moment but also due to its low coercive field. Although the latter is greater than that of permalloy, due to its large magnetocrystalline anisotropy constant and higher magnetostrictive coefficient, it can be tailored by deposition conditions [17].

Related to the growth of FeCo thin films on MgO (001), it is established that FeCo can grow epitaxially on MgO (001) substrates with a 45° rotation between the FeCo and MgO crystal lattices [22,23]. Several bilayers with different FeCo thicknesses were fabricated and characterized, structurally and magnetically, by X-ray diffraction (XRD), Rutherford Backscattering Spectrometry (RBS), Raman spectroscopy, and vectorial Kerr magnetometry (v-MOKE). The latter was used to obtain the angular dependence of the exchange bias, remanence, and coercivity both, as deposited samples and those obtained after the field-cooling process (FC).

2. Materials and Methods

NiO (AF)/ FeCo (F) bilayers were deposited on MgO (001) and Al_2O_3 (0001) substrates by ion beam sputtering using Ar^+ ions from a 3 cm Kaufmann-type ion source in a vacuum chamber with a base pressure of 2×10^{-5} Pa. NiO thin films were obtained from a pure nickel (99.99%) target in a controlled atmosphere of oxygen and argon with P(Ar) = 1.4×10^{-2} Pa and P(O_2) ranging from 0.9 to 2.7×10^{-2} Pa. The substrate temperature during NiO deposition was maintained at 500 °C and the sputter ion energy and current density were 650 eV and 1.1 mA/cm^2. Subsequently, FeCo thin films with thicknesses ranging between 1.5 and 16 nm were obtained from a 99.99% pure FeCo target in an Ar atmosphere with P(Ar) = 1.4×10^{-2} Pa and 200 °C substrate temperature. In this case, the sputter ion energy and current density were 550 eV and 0.8 mA/cm^2, respectively. The substrates were rotated at 2 rpm to increase the homogeneity of the deposited material. In all the cases, a 2 nm Al capping layer was deposited on top of the F layer to prevent oxidation for ex situ studies.

The crystal structure and texture of the different films were analyzed by X-ray diffraction (XRD) in a θ/2θ configuration using a Bruker D8 Discover (Karlsruhe, Germany) system with Cu-Kα radiation.

The in-depth composition and thickness of the different layers were determined by Rutherford Backscattering Spectrometry (RBS) at the CMAM 5 MV tandem accelerator using $^4He^+$ at 1.8 and 3.045 MeV. A silicon barrier detector, at a scattering angle of 170.5°, measured the backscattering ions while a 3-axis goniometer was employed to control the crystal position [24]. The distribution and quantification of the various elements of the different layers of the heterostructures were determined with the SIMNRA simulation software 7.02 package. The thicknesses of the different layers are measured during deposition by a quartz crystal microbalance, while RBS was also employed to accurately determine the thickness of the different layers by using a mass density of 6.67 and 8.40 g/cm^3 for NiO and FeCo films. Figure S1, in Supplementary Materials, shows the RBS spectra and the SIMNRA simulation of 3 NiO/FeCo bilayers grown on MgO (001) substrates with a FeCo thickness of 3, 8, and 16 nm as determined by the microbalance, which is in good agreement with the values obtained in the simulation, i.e., 2.8, 8.0, and 16.5 nm. These results are also shown in Table S1 at the Supplementary Materials. Table S1 also includes the thickness of the corresponding AF NiO layers as well as the composition of FeCo and NiO layers. The measurements were carried out in both random and channeling configurations. If the film grows epitaxially and the direction of the incident $^4He^+$ particles is aligned with a high-symmetry direction of the crystal lattice, most of the incoming ions pass through the channel provided by the empty space available within the crystal lattice and penetrate deep into the material. The resultant decrease in the scattering yield is a measure of the epitaxial quality of the films.

Confocal micro-Raman experiments were carried out on the AF/F bilayers. The measurements were collected using a confocal Raman microscope (CRM) ALPHA 300RA, WITec, Ulm, Germany at room temperature with an Nd:YAG linearly polarized laser (532 nm). The Raman spectra were recorded in the range of 0–3600 cm^{-1}, using an objective with a numerical aperture of 0.95 and a laser excitation power of 3.2 mW to avoid any damage to the films. The Raman signal was collected from the confocal plane of the film with the highest intensity, averaging several Raman spectra from different regions.

The angular dependence of magnetization was investigated at room temperature by high-resolution vectorial-Kerr magneto-optical measurements (v-MOKE) in a longitudinal configuration [25,26]. MOKE hysteresis loops were recorded by changing the in-plane angular orientation of the sample, α_H, keeping the external magnetic field direction fixed. The angular orientation, ranging from 0 to 360◦ was probed at intervals off 9° with a maximum applied magnetic field of 110 mT. The exchange bias is characterized by the so-called exchange bias field, H_e, defined as $H_e = (|H_{c1}|\text{-}|H_{c2}|)/2$ where H_{c1} and H_{c2} are the coercive fields of the ascending and descending branches of the hysteresis loop. H_E is a measure of the hysteresis loop's shift, the fingerprint of exchange bias phenomena. In this

context, the coercive field is defined as $H_c = (|H_{c1}| + |H_{c2}|)/2$, encoding the absolute half width of the loop at the crossing with a 0 magnetization axis, representing the standard definition of the coercive field. A field heating/cooling procedure, FC, was performed in vacuum at P $\approx 10^{-4}$ Pa by heating the system up to 650 K for 10 min, above the Neel temperature of NiO, T_N = 525 K, and then cooling down to room temperature under the presence of an external magnetic field of 300 mT. The field was applied at the easy axis of the as-deposited bilayer previously measured by v-MOKE.

3. Results

Figure 1 shows the XRD pattern of a NiO/FeCo bilayer with a thickness of FeCo (d_{FeCo}) of 16 nm grown on MgO (001) substrate (Figure 1a) and Al_2O_3 (0001) substrate (Figure 1c) highlighting the diffraction peak of the FeCo layer in θ/2θ configuration. The sketch of the bilayer is included in Figure 1b. In Figure 1a, only two peaks can be distinguished in the complete diffractogram. The most intense one at 43.0° corresponds to MgO (200), which completely overlaps with the peak of the NiO (200) plane due to a very close mismatch between both lattices and the peak at 64.2° corresponding to FeCo (200), which indicates that the complete heterostructure grows in the (100) direction. The lattice parameter for the FeCo layer, 0.290 nm, indicates that the FeCo layer grows 45° rotated with respect to the NiO (100) layer to reduce the mismatch to −4.6%, in a similar way to the growth of FeCo on MgO (001) substrates [22,23].

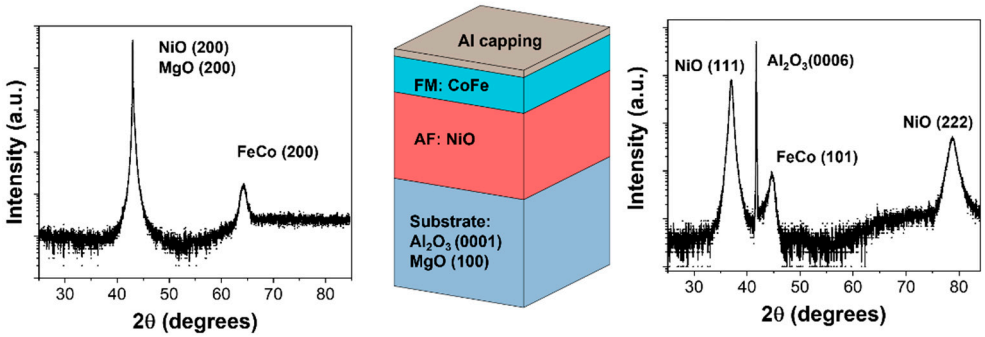

Figure 1. XRD diffraction pattern of NiO/FeCo bilayer with d_{FeCo} = 16 nm on (**a**) MgO (001) and (**c**) Al_2O_3 (0001) substrates. (**b**) Heterostructure arrangement sketched.

Oriented NiO (111) thin films have been grown on c-cut Al_2O_3 substrates and the corresponding diffractogram of the NiO/FeCo bilayer is shown in Figure 1c, in which an intense peak is visible due to the Al_2O_3 (0006) diffraction plane as well as the NiO (111), NiO (222), and FeCo (101) diffraction planes. The lattice mismatch between NiO films and Al_2O_3 substrate has been calculated following the well-known crystallographic orientation relationships and the domain-matching epitaxy proposed by Lee et al. [15], who reported a bi-epitaxial growth with both in-plane relationships: $[\bar{1}10]$ NiO ∥ $[01\bar{1}0]$ Al_2O_3 and $[\bar{1}\bar{1}2]$ NiO ∥ $[2\bar{1}\bar{1}0]$ Al_2O_3. The mismatch value obtained by our NiO thin films, by using the average lattice parameter obtained for all the samples, i.e., 0.422 nm, is 8.6%. We have also obtained a lattice parameter of the FeCo layer of 0.287 nm. To calculate the lattice mismatch of FeCo (110) with respect to NiO (111), we could assume a similar epitaxial relationship to the ones already demonstrated [22,23] during the growth of FeCo(110) on MgO (111) substrates based on the closest crystal structure and lattice parameter between MgO and NiO. It is well established that FeCo (110) bcc thin films grow epitaxially on MgO (111) substrates with two types of domains, Nishiyama–Wassermann domains and Kurdjumov–Sachs domains, with the following relationship: [001] FeCo ∥ $[1\bar{1}0]$ MgO and $[1\bar{1}1]$ FeCo ∥ $[1\bar{1}0]$ MgO [22,23], giving values for the lattice mismatch of −3.8% and −16.7%, respectively, in our bilayers.

The FC process used in this work by heating the bilayers up to 650 K in the presence of a 300 mT magnetic field does not induce significant structural changes in the bilayers. Figure S2, at Supplementary Materials, shows the XRD diffraction patterns of the NiO/FeCo bilayer with d_{FeCo} = 3 nm before and after the FC process, showing any structural change in terms of lattice parameter or crystalline orientation.

The XRD in the θ/2θ configuration does not allow us to completely understand the strains and disorder generated at the interfaces, so we have carried out RBS experiments in a random/channeling configuration to clarify this point. Figure 2 shows the RBS spectra on the random and channeling configuration for a NiO/FeCo bilayer with d_{FeCo} = 2.5 nm, which was grown on MgO (001) substrate (Figure 2a) and on Al_2O_3 (0001) substrate (Figure 2b). The RBS technique is generally used to determine the chemical composition, thickness, and in-depth atomic distribution of the different elements present in the films; however, it can also be used to explore the epitaxial nature of thin films and the disorder generated at the interfaces. Comparing the curves on both heterostructures, it is clear that the yield decreases in the channeling spectra when the (100) NiO-oriented film is aligned with MgO (001) substrate and when the (111) NiO-oriented film is aligned with the Al_2O_3 (0001) substrate, confirming the single-orientation growth on both substrates.

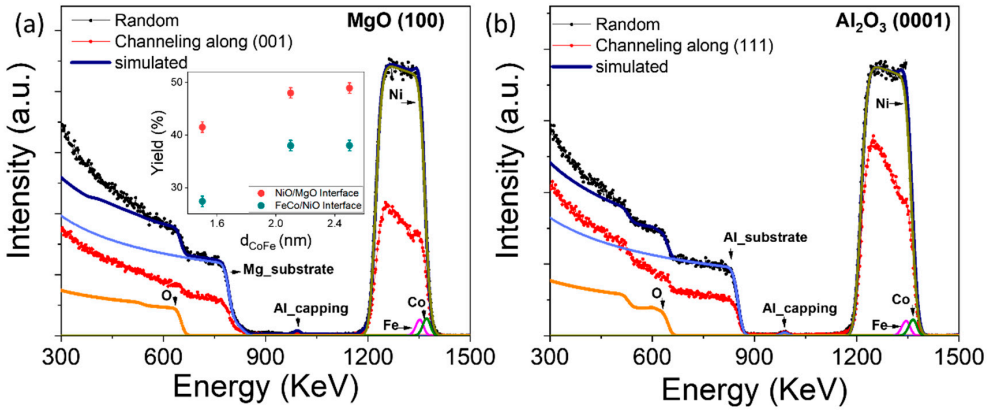

Figure 2. Random and (**a**) (001)-aligned RBS and (**b**) (111)-aligned RBS spectra NiO/FeCo bilayer obtained with ^{4}He+ ions at 1.8 MeV grown on MgO (001) and Al_2O_3 (0001) substrates, respectively. The simulation with the SIMNRA program including the fitting signal for O, Ni, Fe, Co, Mg, and Al is also included.

The ratio between yields of channeling and random spectra can be used as an indicator of the epitaxial or crystalline quality of the deposited layers. The line shape of the RBS/channeling spectrum can indicate the in-depth distribution of the density of defects or the structural disorder in the layers. The RBS/channeling spectrum for the heterostructure grown on MgO (001) substrate shows a yield ratio value at the MgO/NiO interface of 48%, significantly higher than those found near the NiO/FeCo interface, with a minimum yield ratio of 38% indicating a disorder at the MgO/NiO interface generated by strains that relax as the NiO layer is grown. In the inset of the figure, both yields as a function of the FeCo thickness are shown. The minimum values for the smaller thickness of FeCo, i.e., $Yield_{\ interface\ NiO/MgO}$ = 41% and $Yield_{\ minimum\ NiO}$ = 27% can be observed. Similar results but with higher yield values have been obtained for the bilayer grown on Al_2O_3 substrate (d_{FeCo} = 2.5 nm). In this case, the yield ratio at the Al_2O_3/NiO interface reaches a high value of up to 73% while the minimum value is as high as 50% in good agreement with the highest mismatch between the NiO film and the substrate in this case. The relative channeling at the FeCo layer increases, up to 46%, with respect to the minimum value at the NiO/FeCo interface, i.e., 38%, for the MgO substrate. This fact is also observed in the case of Al_2O_3 substrates, in which the yield at the FeCo layer is 63%, which is also higher than the minimum value found at the NiO/FeCo interface, i.e., 50%. This could indicate similar

strains generated during the growth of FeCo on Ni (200) and NiO (111)-oriented layers, confirming the lattice mismatch values at the NiO/FeCo interfaces on both orientations.

In-depth elemental composition and thickness of the different NiO and FeCo layers as well as the Al capping layer were determined by the simulation of the random spectra in terms of O, Ni, Fe, Co, Mg, and Al signals, as shown in Figure 2. Signals for O, Ni, Al, and Fe are included. The estimated composition and thickness for this particular bilayer is $Ni_{0.48}O_{0.52}$ (d = 135 nm)/$Fe_{0.49}Co_{0.51}$ (d = 2.5 nm)/$Al_{0.5}O_{0.5}$ (d = 1.7 nm). Table S1, at the Supplementary Materials, shows these results for other bilayers.

Raman spectroscopy has been widely used to analyze the structural and magnetic characteristics of NiO thin films [27,28]. The active Raman modes of NiO films grown on MgO (001) substrate, shown in Figure 3a as black circles, are in full agreement with previous reports [27,28], confirming the generally good quality of the NiO films. The first-order phonon modes, longitudinal optical (LO), 1P, and transverse optical (TO) are inactive Raman modes in the perfect rock-salt-like structure but can appear due to the rhombohedral lattice distortion and the presence of impurity atoms in the crystal lattice. Their intensity is strongly dependent on the stoichiometric ratio in the lattice. The LO+TO and the 2LO(2P) overtones are identified, as well as the two-magnon mode (2M). The 2LO (2P) Raman mode at 1120 cm^{-1} can be attributed to strains in NiO films while the 2M band (2-magnon mode) at about 1500 cm^{-1} is measurable as a fingerprint of AFM ordering [29–31] originated by the interaction between neighboring (111) Ni^{+2} planes. Comparing the Raman signal for NiO on both substrates (Figure 3b), a different intensity ratio between the 2M band and the 2P band is noted, which is sensitive to the type of NiO domains that appear in the different crystallographic orientations. Lower 2M/2P intensity for NiO (111) grown on Al_2O_3 (0001) substrates than for NiO (200) grown on MgO (001) substrates is observed, which is in good agreement with the results found for NiO (111) and NiO (100) single crystals [32].

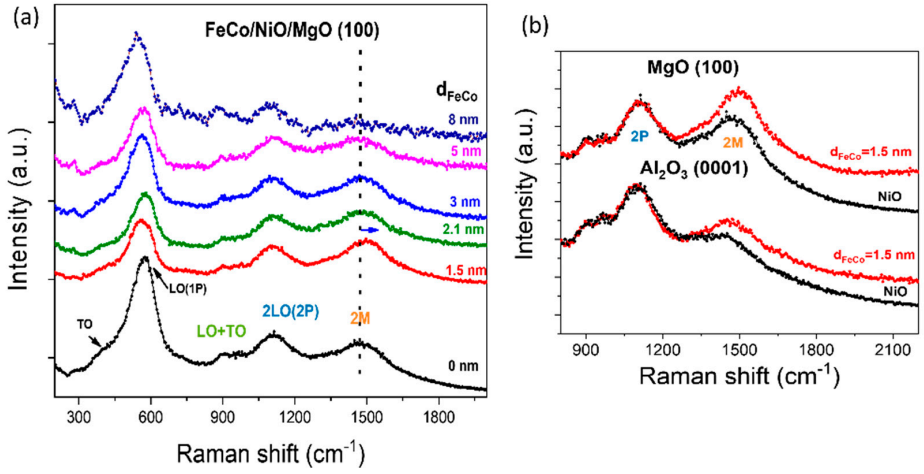

Figure 3. (**a**) Raman spectra of NiO thin films as well as NiO/FeCo bilayers grown on MgO (100) substrates with different FeCo thicknesses as labeled. (**b**) Raman spectra of NiO thin film (black circles) and NiO/FeCo bilayer with d_{FeCo} = 1.5 nm (red circles) grown on MgO (100) and Al_2O_3 (0001) substrates.

Figure 3a also shows the dependence of the Raman active modes of the NiO/FeCo bilayers grown on MgO (001) substrates varying the FeCo thickness. The LO, LO+TO, and 2LO Raman modes are clearly visible in all samples, even for the 8 nm FeCo thickness. For the smallest thickness of the FM layer, i.e., d_{FeCo} = 1.5 nm, a blue shift of 2M mode can be observed along with an increase in its intensity for both substrates (Figure 3b). The evolution of Raman shift and relative intensity of the 2M band has been studied on NiO nanostructures and, in general, both blue shifts and intensity increases are explained by an increase in AFM coupling via Ni-O super-exchange interaction. The light-induced spin–flip interaction known as the next nearest neighboring (NNN) super-exchange interaction

between the Ni^{2+} ions in the linear atomic chains of alternating Ni^{2+} and O^{2-} ions (Ni^{2+}-O^{2-}-Ni^{2+}), in which the oxygen ions are present in the linear atomic chain, mediates the exchange in the NiO crystal lattice. When the crystal symmetry is reduced, the magnon excitation decreases [28].

The 2M excitation is also altered by the FM thickness, which could be influenced by the spin interaction induced by the F layer at the AF/F interface. In order to analyze the intensity of the 2M mode with the FeCo thickness, Raman bands of the bilayers grown on MgO (001) substrates, in which the 2M mode is more intense, were fitted using the Lorentzian function, as is shown in the insets of Figure 4 for 2P and 2M modes. Figure 4 displays the relative intensity between 2M and 2P modes as a function of FeCo thickness obtained from the fitting, showing an increase in the intensity 2M/2P ratio for the smallest thickness as compared with the NiO film, as mentioned above, which decreases as the FeCo thickness increases. This behavior can be an indication of the contribution of the interlayer spins that can be pinned at the AF NiO, modifying the exchange interaction between the Ni^{2+} ions. In any case, to understand this evolution it is necessary to investigate the exchange coupling between the AF and F layers, as we shall do below.

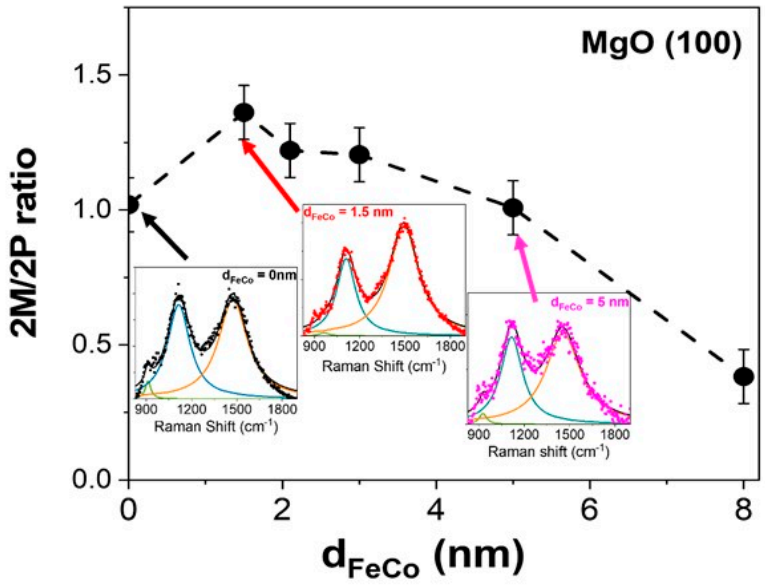

Figure 4. Intensity of 2M/2P and area ratio as a function of FeCo thickness. In the inset, the fitting with the Lorentzian functions of LO+TO, 2LO, and 2M Raman modes for NiO thin film (arrow and symbols black) and for two NiO/FeCo bilayers with d_{FeCo} = 1.5 nm (arrow and symbols red) and d_{FeCo} = 5 nm (arrow and symbols magenta), respectively, is shown.

For the magnetic characterization, we focused on the study of the in-plane magnetic anisotropy for the two bilayer types, using angular-dependent v-MOKE measurements in longitudinal configuration. In this configuration, the external field is applied parallel to the sample plane, and also parallel to the v-MOKE optical plane [25,26]. The magnetization components provided by the vectorial magnetometer are the two in-plane components of the magnetization, one parallel to the external field, and the other one perpendicular to it. By applying an external field ramp from positive to negative values and back, we force the system to reverse its magnetization, and the way this magnetization reverses comprises the so-called reversal process, where both reversible and irreversible paths may appear. The reversible and irreversible pathways of the reversal process manifest in the shape of the curve of magnetization versus external field: the so-called hysteresis loops. Since we obtain two of the magnetization components, we call these loops vectorial hysteresis loops. Each one corresponds to the reversal pathways of the aforementioned components, from which the different magnetic parameters (remanence, saturation, and transition or coercive fields, for instance) can be extracted.

The hysteresis loops are measured for the whole range (360°) of angles of the external field with respect to the sample by rotating the sample around the polar axis (perpendicular to the sample surface), and the evolution with the angle of the different parameters, i.e., the signature of the reversal process, reveals the magnetic symmetries of the system. In Figure 5a,c, the coercive fields and exchange bias fields (H_C and H_E, respectively) are depicted as deposited and FC samples, while in Figure 5b,d they are depicted as the corresponding remanences: in the upper plots (a and b) we see those for the bilayer grown on MgO (001) substrate with d_{FeCo} = 3.0 nm and in the lower plots (c and d) those for the bilayer grown on Al_2O_3 (0001) substrate with d_{FeCo} = 1.5 nm. Since MOKE magnetometry does not provide an absolute value of the magnetization, remanence has been normalized to the saturation magnetization for ease of interpretation. For the NiO/FeCo bilayer grown on MgO (001) substrate, the 0° angle reference has been assigned to the external field applied parallel to the (100) direction.

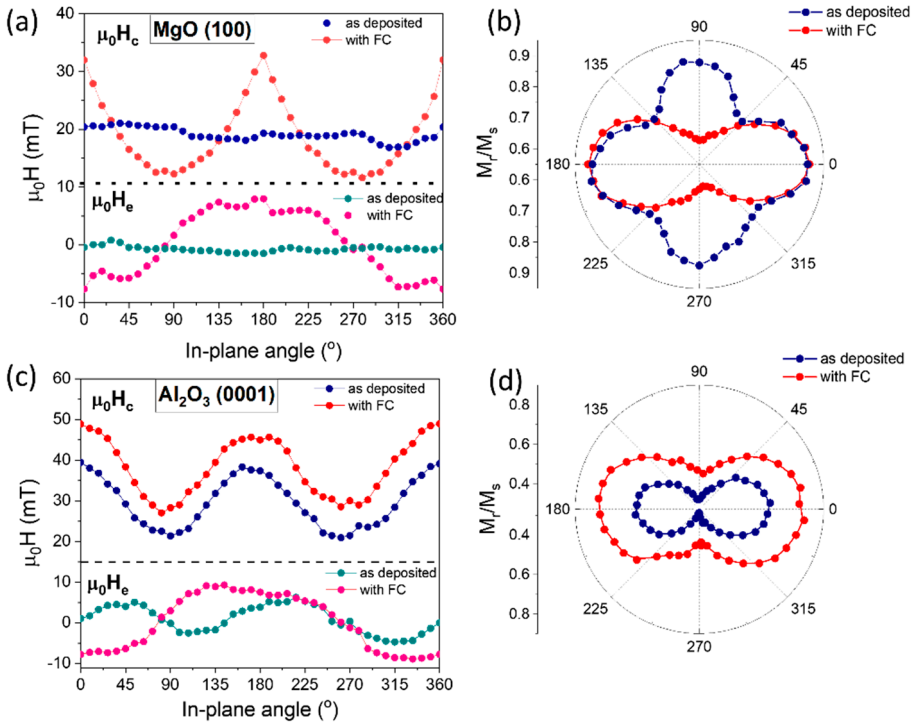

Figure 5. (**a**,**c**) Linear plot of the coercive and exchange bias field as a function of the in-plane angle for NiO/FeCo (d_{FeCo} = 3 nm) grown on MgO (001) substrate and NiO/FeCo (d_{FeCo} = 1.5 nm) grown on Al_2O_3 (0001) substrate. The dashed black lines are to clarify the evolution of H_c and H_e separately. (**b**,**d**) Polar plots of M_r/M_s for the bilayers grown on MgO (001) and Al_2O_3 (0001) substrates, respectively.

We first examine the NiO/FeCo bilayer grown on MgO (001) substrate with d_{FeCo} = 3.0 nm. This thickness has been chosen to completely saturate the magnetization at the largest field available in our v-MOKE setup, i.e., 110 mT. For the as-deposited sample, while remanence exhibits a four-fold symmetry, H_c exhibits a two-fold symmetry. This is an indication of coexistence/competition between biaxial anisotropy with a rather small contribution of collinear uniaxial anisotropy. Since the remanence is measured in a reversible region of the reversal process, it is sensible to the predominant magnetic anisotropy, while weaker contributions may be obscured by this. On the other hand, the weaker uniaxial anisotropy manifests more clearly in the irreversible region, where H_C is measured. However, the analysis of this kind of magnetic anisotropy competition is complex. A detailed model system with competing anisotropies can be found in [33,34].

The origin of the predominant biaxial anisotropy of this bilayer can be straightforwardly attributed to magnetocrystalline anisotropy induced on FeCo by the epitaxial

growth of the NiO layer on the MgO (001) substrate. After the field cooling process in the presence of the 300 mT applied field along the (100) direction, the uniaxial contribution becomes larger and biased, as can be seen now even in the remanence (Figure 5b, red circles), dominating the four-fold contribution. The exchange bias (EB) field, H_E, appears with one-fold symmetry, as can be seen in Figure 5a, but preserves the axis direction of the two-fold contribution. H_e is very low (≈1 mT) and increases up to 7.8 mT after FC, showing clearly the unidirectional anisotropy induced by the FC process. At 0°, the negative H_e value indicates that the shift of the hysteresis loop takes place in the opposite direction of the static magnetic field applied direction during the FC process, which is the typical negative exchange bias effect [6]. The coercive field at the easy axis also increased considerably after the FC process from 18.9 mT to 33.1 mT, showing again the strong uniaxial anisotropy originated by the FC process that dominates the four-fold magnetocrystalline anisotropy observed on the as-deposited bilayer. Interestingly, the coercive field behavior radically changes in the FC sample with respect to the as-deposited one: while in the as-deposited sample the H_C presents the maxima as large plateaus, typical of reversal process based on nucleation of magnetic domains and domain wall propagation, i.e., propagative process, in the FC sample they become stepped curves typical of the macrospin reversal process or nucleative process. This is expected for magnetic nanoparticles, but it is also reported for systems with extremely small magnetic domains. Indeed, this is also a common situation for EB systems, and the behavior is well described in the framework of the Stoner–Wohlfarth model (SW) [35,36]. In other words, EB promotes smaller domain sizes in the reversal process to such an extent that the behavior becomes SW-like. This behavior in an extended system (i.e., not a nanoparticle), in which magnetic domains are expected but whose behavior mimics that of a single particle or macrospin instead, is linked to dynamical effects when nucleation is the dominant reversal process.

In the case of the bilayer grown on Al_2O_3 (0001) substrate corresponding to NiO (111) orientation and with a d_{FeCo} = 1.5 nm, it is possible to observe two-fold magnetic anisotropy both in the as-deposited bilayer and after the FC process applied along the easy axis of the as-deposited bilayer. The angular dependences of the remanence and coercive field for the as-deposited bilayer displayed in Figure 5c,d, showing the two-fold magnetic anisotropy, are enhanced after the FC process along the easy axis of the as-deposited bilayer, as expected. A two-fold behavior can also be observed in the exchange bias of the as-deposited bilayer with a maximum value of 4.6 mT. This is not so common but it has been observed in other AF/F bilayers, where the effect was related to microstructural, morphological, and texture effects [6,37,38]. This value increases until 9 mT after the FC process, which is significantly lower with respect to the value found in the bilayer grown on MgO (001) substrate for the same FeCo thickness (d_{FeCo} = 1.5 nm) in which $\mu_0 H_e$ = 20 mT. Moreover, the magnetization was not completely saturated for the bilayer grown on the MgO (001) substrate.

In order to emphasize the differences between both substrates, we have compared in Figure 6 the magnetic properties of NiO/FeCo (d_{FeCo} = 5 nm) bilayers grown on MgO (001) and Al_2O_3 (0001) substrates. Figure 6a–c shows the hysteresis loops at the easy axis before and after FC, the angular dependence of the coercive field and the absolute value of the exchange bias, and the longitudinal and transversal component of the magnetization at the easy and hard axis after the FC process for the bilayer grown on MgO (001) substrate, while Figure 6d–f shows the corresponding ones for the bilayer grown on Al_2O_3 (0001) substrate. The in-plane hysteresis loop at the easy axis (e.a.) for the as-deposited bilayer grown on MgO (001) substrate (black circles on Figure 6a), presents a complex shape at the transition, probably originated by pining effects between ferromagnetic domains and the underlying antiferromagnetic domain texture of the NiO, resulting in some domains pinned in one direction and the others in the opposite direction. This effect was previously reported for other AF/F systems as NiMn/Co bilayers [37]. After the FC process, the double loop disappears (Figure 6a, red circles) due to the induced strong uniaxial anisotropy combined with the increase in the coercive and exchange bias field. However, these effects are not

observed in the bilayer grown on Al_2O_3 (0001) substrates in which the hysteresis loops before and after FC (Figure 6d) are very similar, indicating the exchange coupling is larger for the NiO (200) texture than the NiO (111) texture. Similar and unpredicted behavior, assigned to the contribution of the interface roughness, has been observed on NiO/NiFe bilayers since the spin structure of NiO (200) planes is predicted to be compensated while the (111) planes are uncompensated [39].

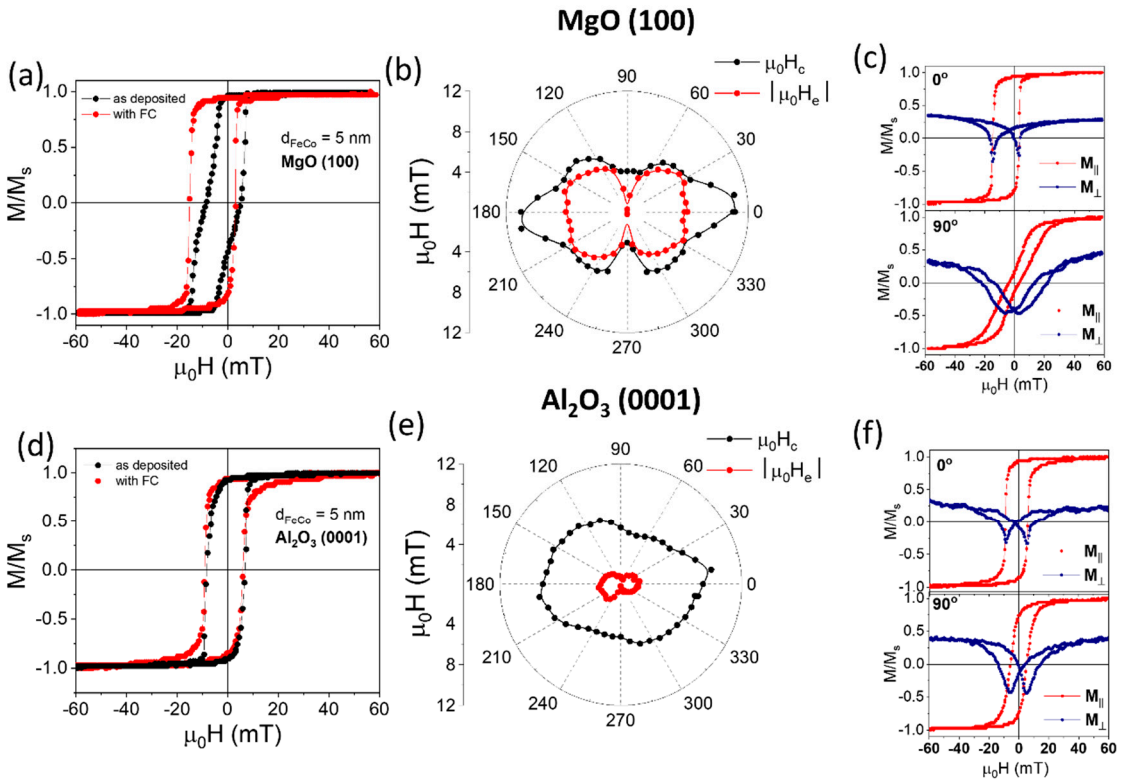

Figure 6. (**a**,**d**) Hysteresis loops at the easy axis of the NiO/FeCo (d_{FeCo} = 5 nm) bilayer as grown (black circles) and after FC process (red circles), (**b**,**e**) polar plots of the coercive field (black circles) and absolute value of exchange bias (red circles) after FC process and (**c**,**f**) hysteresis loop for the $M_{||}$ and the $M_\perp$ components as labeled on the magnetization at the easy axis (0° in-plane angle) and hard axis (90° in-plane angle) after FC process of the bilayer grown on MgO (001) (**c**) and Al_2O_3 (0001) (**f**) substrates, respectively.

Polar plots of H_c and the absolute value of H_e after the FC process for the bilayer grown on MgO (001) and Al_2O_3 (0001) substrates are shown in Figure 6b,e, respectively, emphasizing the aforementioned differences. For NiO/FeCo grown on MgO (001), the polar plot of H_c and the absolute value of H_e shows the same 2-fold symmetry with the maximum values along the FC direction (100), i.e., 11.7 mT and 6.6 mT for $\mu_0 H_c$ and $\mu_0 H_e$, respectively. However, the bilayer grown on the Al_2O_3 (0001) substrate shows an asymmetric shape for H_c and absolute values of H_e as low as 2 mT in the FC direction, which is a similar value to the one found at the easy axis of the as-deposited bilayer.

In Figure 6c,f, vectorial resolved hysteresis loops after FC are shown for 2 selected directions: 0° and 90°. While at 0° the in-plane parallel component exhibits an almost vertical irreversible transition for both substrates, at 90° the slope is softened, indicative of a hard axis, confirming the symmetries. The perpendicular components also present more abrupt transitions in the case of 0° than in the case of 90°. In all cases shown in Figure 6c,f, the perpendicular saturation (i.e., the perpendicular component of the in-plane magnetization saturation vector, $M_\perp$) does not cross the horizontal axis, which is an indication that the magnetization vector cannot fully reverse to the exact opposite direction upon completely switching off the external field. This asymmetry is also a typical behavior

of EB systems. In addition, the $M_{\perp}$ value in the forward and backward branches of the loop is not the same, resulting in an asymmetry of the total magnetization saturation (modulus of the magnetization vector at saturation). This asymmetry arises from the net magnetic moment being larger in the FC direction than in the other one, due to the contribution of the AF uncompensated magnetic moments at the interface.

One important finding in exchange bias systems is that the exchange bias varies approximately inversely with the thickness of the FM layer [6], a dependence that has also been observed and predicted on the coercive field [40–42]. Figure 7a illustrates the dependence of the coercive field in the as-deposited bilayer as a function of FeCo thickness for the bilayers grown on both substrates, showing a rapid decrease in the coercive field with thickness. A fit of this curve to an inverse function of the thickness is shown in the inset of Figure 7a, resulting in straight lines in good agreement with the predicted functional law, except for an unmatched point corresponding to the smaller thickness of FeCo, i.e., 1.5 nm. The dependence of H_c with the inverse of ferromagnetic layer thickness has been predicted theoretically [40] and observed experimentally [41]. According to Tang et al. [42], it is attributed to an interfacial effect due to induced anisotropies by the exchange coupling. On the contrary, we have not found a dependence of the spontaneous exchange bias with the FeCo thickness, keeping low exchange bias values for the bilayer grown on both substrates (Figure 7b).

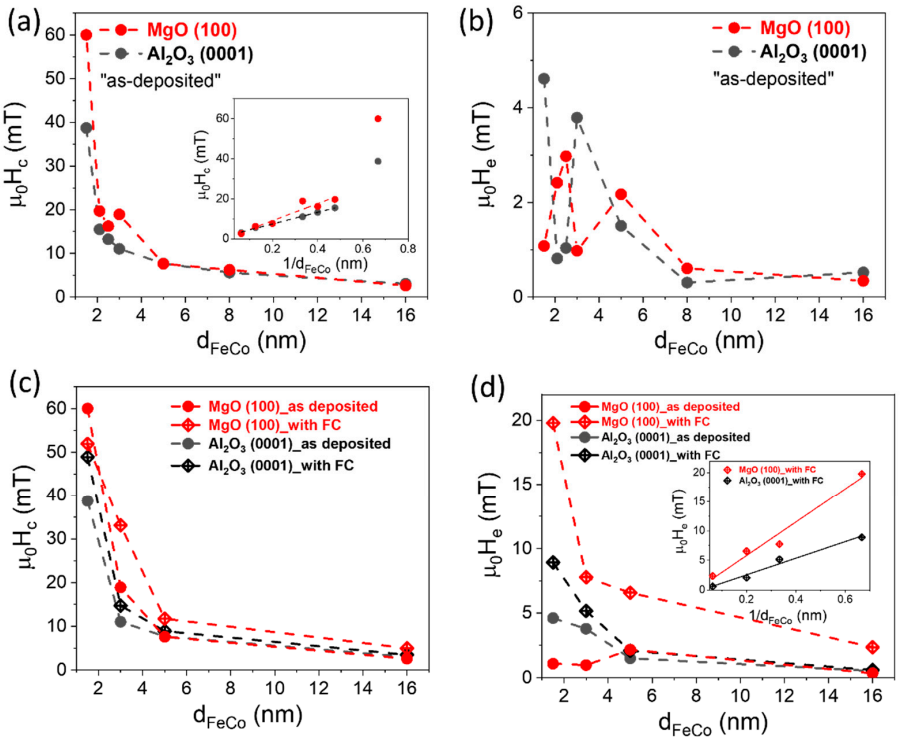

Figure 7. (**a**) Dependence of the coercive as a function of FeCo thickness in the as-deposited bilayers (inset versus inverse thickness) (**b**) Exchange bias as a function of thickness in the as-deposited bilayers. Comparison of the coercive field (**c**) and the exchange field (**d**) for the as deposited and FC bilayers. In the inset of (**d**), the expected dependence of H_e after FC with the inverse of thickness is included.

The H_c comparison between the as deposited bilayers and after the FC process is shown on Figure 7c, in which an increase in the coercive field values after the FC process can be observed in both substrates in correspondence with an increasing exchange coupling. Finally, in Figure 7d the exchange bias field for the as-deposited and FC bilayers as a function of FeCo thickness is shown, in which an important increment of the H_E after the FC process is observed, which is significantly higher for the bilayers grown on MgO

(001) substrates, i.e., FeCo deposited on NiO (200)-textured films. In the inset of Figure 7d, the expected dependence of the exchange bias with the inverse of the FeCo thickness is shown [6]:

$$H_E = \frac{J_{int}}{M_{FM} d_{FM}}$$

where J_{int} is the unidirectional magnetic interface energy, and M_{FM} and d_{FM} are the magnetization and the thickness of the FM layer, respectively [6].

We can conclude that the exchange coupling is clearly enhanced on NiO (200)-texture based-bilayers grown on MgO (001) substrates; even the NiO (200) shows a compensated spin structure. This fact is also observed with small changes in the deposition condition of the NiO layer.

In order to test this, we have grown NiO/FeCo bilayers with d_{FeCo} = 2.5 nm on MgO (001) and Al_2O_3 (0001) substrates, by using different oxygen partial pressures for the NiO layer, 2.8 × 10^{-2} Pa, which is the one used on the previous results, and 1.6 and 0.9 × 10^{-2} Pa to introduce oxygen vacancies to the NiO layer. To quantify the oxygen concentration in the NiO layer, we have carried out RBS measurements with 3.045 MeV energy $^4He^+$ ions that resonantly enhanced the scattering cross-section of oxygen atoms, as is represented in Figure 8a. For the simulation, we used the $^{16}O(^4He,^4He)^{16}O$ elastic-scattering cross-sections reported by Demarche et al. [43]. The differences in oxygen content between the different NiO layers remain in the detection error of the technique, where the same oxygen composition for all the NiO layers is obtained, i.e., $Ni_{0.48}O_{0.52}$, after simulation. However, an enhanced coercivity can be observed when the NiO/FeCo bilayer grows on the MgO (001) substrate, as the oxygen partial pressure decreases (Figure 8b) while undetectable changes are observed when the bilayer grows on the Al_2O_3 (0001) substrate. In Figure 8c,d, the hysteresis loops at the e.a. for the bilayers grown on MgO (001) and Al_2O_3 (0001) substrates, respectively, clearly show this result, again indicating a high exchange coupling for NiO (200)-texture-based bilayers, but also that the exchange coupling could be controlled by NiO deposition conditions, preferentially on this NiO orientation.

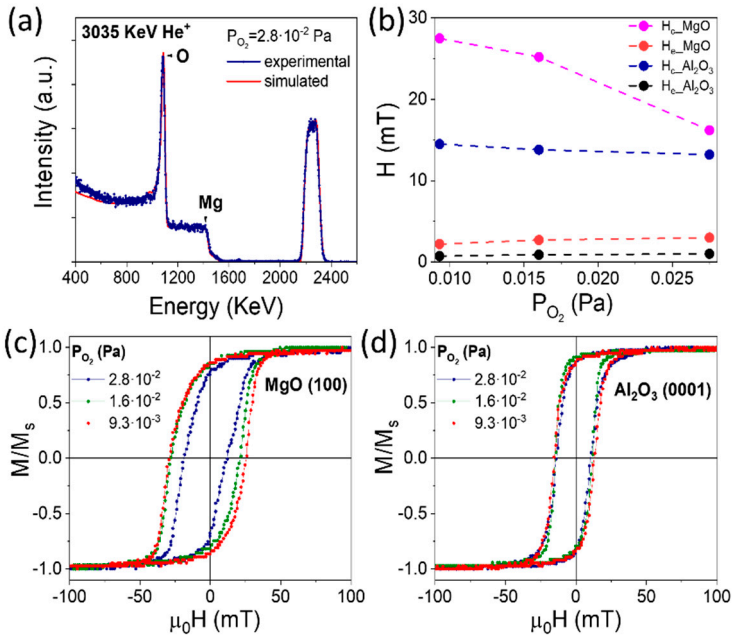

Figure 8. (**a**) RBS spectrum of the NiO/FeCo bilayer grown on MgO (001) substrates with d_{FeCo} = 2.5 nm and P_{O2} = 2.8 × 10^{-2} Pa obtained $^4He^+$ ions with 3.045 MeV energy, and its simulation. (**b**) Dependence of the coercive and exchange bias fields as a function of oxygen partial pressure; (**c**,**d**) hysteresis loops at the e.a. for the bilayers grown on MgO (001) and Al_2O_3 (0001) substrates, respectively.

4. Discussion

Different models have been proposed to explain the exchange coupling mechanism in which the pinned interfacial spin at the AF/F interface and the AF domain wall and interfacial coupling energies are the main factors. The interface roughness is also an important parameter, although in most models its influence on the exchange bias is not fully understood. Typically, quite flat interfaces of AF films result in a small exchange bias, while rougher interfaces show an increased exchange bias; however, the opposite behavior has also been reported [7]. Another factor that is not fully understood is the influence of uncompensated spin at the AF/F interface, which depends on the texture of the AF layer [7].

Here, one of the findings in the as-deposited bilayers is the increase in the coercive field with the inverse of FeCo thickness. The slope of the curve is high when FeCo grows on NiO (200)-textured surfaces as compared to when it grows on Ni (111)-textured surfaces (Figure 7a). This behavior is expected when considering an exchange coupling located at the interface, indicating higher exchange coupling on NiO (200) surfaces, a result that is confirmed by the exchange bias values obtained after FC (Figure 7d) comparing both NiO-texture-based bilayers. All the models predict that the interface coupling retrains the motion of the magnetic domain boundaries and opposes the switching of the F layer, increasing its coercivity. However, the exchange coupling on the spin-unbalanced NiO (111) surface with respect to the balanced one, the NiO (200) surface, should be very different, but the expected behavior is a higher exchange coupling for the bilayers grown on unbalanced NiO (111) surfaces [44], contrary to our results. The higher exchange coupling observed on NiO (200)-texture-based bilayers indicates that other contributions, apart from the spin structure, are relevant in the exchange coupling. Such contribution could be, for instance, interface roughness, interdiffusion, or formation of mixing phases at the interface. In fact, Shen et al. [39] attribute the lower exchange coupling observed on NiO (111)/FeNi bilayers with respect to NiO (200)/FeNi bilayers, similar to our results, to the interface roughness. We have found higher lattice mismatch and higher disorder at the Al_2O_3 (0001)/NiO interface with respect to the ones at MgO (001)/NiO interface. However, we do not have enough information about the NiO/FeCo interfaces and further studies need to be conducted to fully understand the role of the structural quality of the NiO/FeCo interface as well as its compositions in the exchange coupling. In this regard, the deviation of the $1/t_{FM}$ behavior of the coercive field for the as-deposited bilayer with the lowest FeCo thickness, i.e., 1.5 nm, could also be related to morphological effects at the interface. For Fe ultrathin films, when the Fe grains are not connected, Luches et al. [18] have reported a non-ferromagnetic behavior [18]. However, since we have observed ferromagnetism for all FeCo thicknesses, we expect to have a continuous FeCo layer even for the lowest FeCo thickness. We suspect that other effects such as interface roughness or the contribution of a partially oxidized interlayer, more important for the lowest thickness, are contributing to the exchange coupling. Again, to confirm this, further studies about the composition and quality of the interface need to be carried out.

The correlation of the 2M/2P Raman modes intensities, which decrease with the F layer thickness in a similar trend as the coercive field and exchange bias after FC, indicates that the super-exchange interaction of Ni^{2+} ions in the linear atomic chains (Ni^{2+}-O^{2-}-Ni^{2+}) is modified by the pinned interfacial moments. This behavior, which has not been previously reported, indicates that the Raman technique could be appropriated to explore the exchange couplings in AF/F bilayers based on AFMs with active Raman bands.

Another question that needs to be addressed is the spontaneous exchange bias found on some bilayers. In most of the AF/F systems, field cooling is essential to observe exchange coupling and only a few systems having exchange bias without field cooling have been reported [18,44]. This effect, which is not fully understood at this moment [18,44], is attributed to microstructural and morphological properties or texture effects. In our case, the spontaneous exchange bias does not seem to depend on the crystalline orientation of

the NiO surface and on the thickness of the FeCo layer, which is deduced from the random behavior of H_E as a function of the thickness of the FeCo layer (Figure 7b).

5. Conclusions

NiO/FeCo antiferromagnetic/ferromagnetic bilayers with FeCo thickness ranging from 1.5 to 16 nm grown on MgO (001) and Al_2O_3 (0001) substrates have been studied in this work. We have determined a highly oriented NiO layer depending on the substrate used, i.e., NiO (200) and NiO (111) for MgO (001) and Al_2O_3 (0001) substrates, respectively, but higher lattice mismatch and disorder are found at the Al_2O_3 (0001)/NiO interface. High exchange coupling, in terms of high transition field and high exchange bias field after FC, have been obtained for both NiO (200) and NiO (111)-based bilayers, indicating their potential for spintronic applications. For the smaller FeCo thickness, i.e., 1.5 nm, coercive values as high as 60 mT and 49 mT, and exchange bias field values as high as 20 mT and 9 mT have been found on the bilayers grown on MgO (001) and Al_2O_3 (0001) substrates, respectively. The higher exchange coupling of NiO (200)-based bilayers with respect to the NiO (111)-based bilayers is observed for all FeCo thicknesses. This unexpected behavior due to the balanced NiO (200) surface with respect to the unbalanced NiO (111) needs to be addressed in further works focused on structural and morphological studies of the NiO/FeCo interfaces. In the as-deposited bilayers, the competition between magnetocrystalline anisotropy and unidirectional anisotropy due to AF/F exchange coupling can be observed. After FC, the uniaxial contribution becomes larger, dominating the magnetocrystalline anisotropy. The expected reduction in the coercive field and exchange bias field after FC with the thickness of the F layer, observed in the NiO/FeCo bilayers, seems to be related to the behavior of the 2M/2P Raman mode intensity ratio with FeCo thickness.

Supplementary Materials: The following supporting information can be downloaded at: https://www.mdpi.com/article/10.3390/cryst14040369/s1, Figure S1: Random RBS spectra and its simulation with SIMNRA program of NiO/FeCo bilayers with FeCo thickness of (a) 3 nm, (b) 8 nm and (c) 16 nm, obtained with ^{4}He+ ions at 1.8 MeV grown on MgO (001) substrates, respectively.; Table S1: Thickness and composition of NiO and FeCo layers determined by RBS and SIMNRA simulation.; Figure S2: XRD diffraction pattern of NiO/FeCo bilayer with d_{FeCo} = 3 nm on (a) MgO (001) and (b) Al_2O_3 (0001) substrates before and after FC.

Author Contributions: Conceptualization, P.P.; methodology, I.L.-F., C.H.-G., A.S., J.L.F.C. and P.P.; software, I.L.-F.; validation, A.S., J.L.F.C. and P.P.; formal analysis, I.L.-F. and C.H.-G.; investigation, I.L.-F., C.H.-G., A.S., J.L.F.C. and P.P.; data curation, I.L.-F.; writing—original draft preparation, A.S., J.L.F.C. and P.P.; supervision, P.P.; project administration, P.P.; funding acquisition, P.P. and A.S. All authors have read and agreed to the published version of the manuscript.

Funding: The work in Madrid was supported by the Spanish Ministry of Science and Innovation (PID2021-124585NBC32, TED2021-130196B-C22) and Consejería de Educación e Investigación de la Comunidad de Madrid (NANOMAGCOST-CM Ref. P2018/NMT-4321) grants. A.S. acknowledges financial support from PID2021-124585NB-C33 funded by MCIN/AEI/10.13039/501100011033, by "ERDF A way of making Europe", by Project TED2021-130957B-C51 funded by MCIN/AEI/10.13039/501100011033, by the "European Union NextGenerationEU/PRTR" from grant RYC2021-031236-I funded by MCIN/AEI/10.13039/501100011033, and by the "European Union NextGenerationEU/PRTR". J.L.F.C acknowledges financial support from IMDEA nanociencia as well as from project SOnanoBrain (MINECO, PID2020-116181RB-C31).

Data Availability Statement: The raw data supporting the conclusions of this article will be made available by the authors on request.

Acknowledgments: J.L.F.C acknowledges mentor and thesis Julio Camarero.

Conflicts of Interest: The authors declare no conflict of interest.

References

1. Baltz, V.; Manchon, A.; Tsoi, M.; Moriyama, T.; Ono, T.; Tserkovnyak, Y. Antiferromagnetic spintronics. *Rev. Mod. Phys.* **2018**, *90*, 015005. [CrossRef]
2. Jungwirth, T.; Marti, X.; Wadley, P.; Wunderlich, J. Antiferromagnetic spintronics. *Nat. Nanotechnol.* **2016**, *11*, 231–241. [CrossRef] [PubMed]
3. Kampfrath, T.; Sell, A.; Klatt, G.; Pashkin, A.; Mährlein, S.; Dekorsy, T.; Wolf, M.; Fiebig, M.; Leitenstorfer, A.; Huber, R. Coherent terahertz control of antiferromagnetic spin waves. *Nat. Photonics* **2010**, *5*, 31–34. [CrossRef]
4. Moriyama, T.; Hayashi, K.; Yamada, K.; Shima, M.; Ohya, Y.; Ono, T. Intrinsic and extrinsic antiferromagnetic damping in NiO. *Phys. Rev. Mater.* **2019**, *3*, 051402. [CrossRef]
5. Lebrun, R.; Ross, A.; Bender, S.A.; Qaiumzadeh, A.; Baldrati, L.; Cramer, J.; Brataas, A.; Duine, R.A.; Kläui, M. Tunable long-distance spin transport in a crystalline antiferromagnetic iron oxide. *Nature* **2018**, *561*, 222–225. [CrossRef] [PubMed]
6. Nogués, J.; Schuller, I.K. Exchange bias. *J. Magn. Magn. Mater.* **1999**, *192*, 203–232. [CrossRef]
7. Blachowicz, T.; Ehrmann, A. Exchange bias in thin—An update. *Coatings* **2021**, *11*, 122. [CrossRef]
8. Chappert, C.; Fert, A.; Van Dau, F.N. The emergence of spin electronics in data storage. *Nat. Mater.* **2007**, *6*, 813–823. [CrossRef]
9. Bommanaboyena, S.P.; Backes, D.; Veiga, L.S.I.; Dhesi, S.S.; Niu, Y.R.; Sarpi, B.; Denneulin, T.; Kovács, A.; Mashoff, T.; Gomonay, O.; et al. Readout of an antiferromagnetic spintronics system by strong exchange coupling of Mn2Au and Permalloy. *Nat. Commun.* **2021**, *12*, 6539. [CrossRef]
10. Rongione, E.; Gueckstock, O.; Mattern, M.; Gomonay, O.; Meer, H.; Schmitt, C.; Ramos, R.; Kikkawa, T.; Mičica, M.; Saitoh, E.; et al. Emission of coherent THz magnons in an antiferromagnetic insulator triggered by ultrafast spin–phonon interactions. *Nat. Commun.* **2023**, *14*, 1818. [CrossRef]
11. Arai, K.; Okuda, T.; Tanaka, A.; Kotsugi, M.; Fukumoto, K.; Ohkochi, T.; Nakamura, T.; Matsushita, T.; Muro, T.; Oura, M. Three-dimensional spin orientation in antiferromagnetic domain walls of NiO studied by x-ray magnetic linear dichroism photoemission electron microscopy. *Phys. Rev. B* **2012**, *85*, 104418. [CrossRef]
12. Weber, N.B.; Ohldag, H.; Gomonaj, H.; Hillebrecht, F.U. Magnetostrictive Domain Walls in Antiferromagnetic NiO. *Phys. Rev. Lett.* **2003**, *91*, 237205. [CrossRef]
13. Slack, G.A. Crystallography and domain walls in antiferromagnetic NiO crystals. *J. Appl. Phys.* **1960**, *31*, 1571. [CrossRef]
14. Lindahl, E.; Lub, J.; Ottosson, M.; Carlsson, J.O. Epitaxial NiO(100) and NiO(111) films grown by atomic layer deposition. *J. Cryst. Growth* **2009**, *311*, 4082–4088. [CrossRef]
15. Lee, J.H.; Kwon, Y.H.; Kong, B.H.; Lee, J.Y.; Cho, H.K. Biepitaxial growth of high-quality semiconducting NiO thin films on (0001) Al_2O_3 substrates: Microstructural characterization and electrical properties. *Cryst. Growth Des.* **2012**, *12*, 2495–2500. [CrossRef]
16. Becker, M.; Polity, A.; Klar, P.J. NiO films on sapphire as potential antiferromagnetic pinning layers. *J. Appl. Phys.* **2017**, *122*, 175303. [CrossRef]
17. Yang, W.; Liu, J.; Yu, X.; Wang, G.; Zheng, Z.; Guo, J.; Chen, D.; Qiu, Z.; Zeng, D. The Preparation of High Saturation Magnetization and Low Coercivity Feco Soft Magnetic Thin Films via Controlling the Thickness and Deposition Temperature. *Materials* **2022**, *15*, 7191. [CrossRef] [PubMed]
18. Luches, P.; Benedetti, S.; di Bona, A.; Valeri, S. Magnetic couplings and exchange bias in Fe/NiO epitaxial layers. *Phys. Rev. B* **2010**, *81*, 054431. [CrossRef]
19. Slezak, M.; Nayyef, H.; Drózdz, P.; Janus, W.; Swierkosz, E.; Szpytma, M.; Zajaz, M.; Koziol-Rachwal, A.; Slezak, T. Memory of frozen and rotatable antiferromagnetic spins in epitaxial CoO(111)/Fe and NiO(111)/Fe bilayers. *Nucl. Inst. Methods Phys. Res. B* **2023**, *539*, 148–151. [CrossRef]
20. Zhang, Y.; Zhang, W.; Li, J.; Ren, Y.; Ni, J.; Lin, Y.; Xu, D.; Zhang, X.; Dai, B. Annealing temperature dependence of non-collinear magnetic anisotropy in NiFe/NiO bilayers. *J. Magn. Magn. Mater.* **2021**, *539*, 168401. [CrossRef]
21. Dekadjevi, D.T.; Jaoueb, T.; Spenato, D.; Pogossian, S.P.; Youssef, B. Experimental evidences and driving mechanisms for anisotropic misalignments in exchange coupled systems. *Eur. Phys. J. B* **2011**, *80*, 121–125. [CrossRef]
22. Nishiyama, T.; Ohtake, M.; Kirino, F.; Futamoto, M. Preparation and structural characterization of FeCo epitaxial thin films on insulating single-crystal substrates. *J. Appl. Phys.* **2010**, *105*, 107. [CrossRef]
23. Shikada, K.; Ontake, M.; Kirino, F.; Futamoto, M. Microstructure and magnetic properties of FeCo epitaxial thin films grown on MgO single-crystal substrates. *J. Appl. Phys.* **2009**, *105*, 07C303. [CrossRef]
24. Redondo-Cubero, A.; Borge, M.J.G.; Gordillo, N.; Gutiérrez, P.C.; Olivares, J.; PérezCasero, R.; Ynsa, M.D. Current status and future developments of the ion beam facility at the centre of micro-analysis of materials in Madrid. *Eur. Phys. J. Plus* **2021**, *136*, 175. [CrossRef]
25. Jiménez, E.; Mikuszeit, N.; Cuñado, J.L.F.; Perna, P.; Pedrosa, J.; Maccariello, D.; Rodrigo, C.; Niño, M.A.; Bollero, A.; Camarero, J.; et al. Vectorial Kerr magnetometer for simultaneous and quantitative measurements of the in-plane magnetization components. *Rev. Sci. Instrum.* **2014**, *85*, 053904. [CrossRef] [PubMed]
26. Cuñado, J.J.F.; Pedrosa, J.; Ajejas, F.; Bollero, A.; Perna, P.; Terán, F.J.; Miranda, R.; Camarero, J. Vectorial-magneto optical Kerr effect technique combined with variable temperature and full angular range all in a single setup. *Rev. Sci. Instrum.* **2015**, *86*, 04109. [CrossRef] [PubMed]
27. Aytan, E.; Debnath, B.; Kargar, F.; Barlas, Y.; Lacerda, M.M.; Li, J.X.; Lake, R.K.; Shi, J.; Balandin, A.A. Spin-phonon coupling in antiferromagnetic nickel oxide. *Appl. Phys. Lett.* **2017**, *111*, 252402. [CrossRef]

28. Sunny, A.; Balasubramanian, K. Raman Spectral Probe on Size-Dependent Surface Optical Phonon Modes and Magnon Properties of NiO Nanoparticles. *J. Phys. Chem. C* **2020**, *124*, 12636–12644. [CrossRef]
29. Feldl, J.; Budde, M.; Tschammer, C.; Bierwagen, O.; Ramsteiner, M. Magnetic characteristics of epitaxial NiO films studied by Raman spectroscopy. *J. Appl. Phys.* **2020**, *127*, 235105. [CrossRef]
30. Bala, N.; Singh, H.K.; Verma, S.; Rath, S. Magnetic-order induced effects in nanocrystalline NiO probed by Raman spectroscopy. *Phys. Rev. B* **2020**, *102*, 024423. [CrossRef]
31. Massey, M.J.; Chen, N.H.; Allen, J.W.; Merlin, R. Pressure dependence of two-magnon Raman scattering in NiO. *Phys. Rev. B* **1990**, *42*, 8776. [CrossRef] [PubMed]
32. Nina Mironova-Ulmane, N.; Kuzmin, A.; Sildos, I.; Pärs, M. Polarisation dependent Raman study of single-crystal nickel oxide. *Cent. Eur. J. Phys.* **2011**, *9*, 1096–1099.
33. Cuñado, J.L.F.; Pedrosa, J.; Ajejas, F.; Perna, P.; Miranda, R.; Camarero, J. Direct observation of temperature-driven magnetic symmetry transitions by vectorial resolved MOKE magnetometry. *J. Phys. Condens. Matter* **2017**, *29*, 405804.
34. Cowburn, R.P.; Gray, S.J.; Ferré, K.; Bland, J.A.C.; Miltat, J. Magnetic switching and in-plane uniaxial anisotropy in ultrathin Ag/Fe/Ag(100) epitaxial films. *J. Appl. Phys.* **1995**, *78*, 7210. [CrossRef]
35. Cuñado, J.L.F.; Bollero, A.; Pérez-Castañeda, T.; Perna, P.; Ajejas, F.; Pedrosa, J.; Gudín, A.; Maldonado, A.; Niño, M.A.; Guerrero, R.; et al. Emergence of the Stoner-Wohlfarth astroid in thin films at dynamic regime. *Sci. Rep.* **2017**, *7*, 13474. [CrossRef] [PubMed]
36. Stoner, E.C.; Wohlfarth, E.P. A mechanism of magnetic hysteresis in heterogeneous alloys. *Philos. Trans. R. Soc. Lond. Ser. A* **1948**, *240*, 599. [CrossRef]
37. Akbulut, A.; Akbulut, S.; Yildiz, F. Origin of spontaneous exchange bias in Co/NiMn bilayer structure. *J. Magn. Magn. Mater.* **2016**, *417*, 230–236. [CrossRef]
38. Tsai, C.Y.; Hsu, J.H.; Saravanan, P.; Lin, K.F. Study on the occurrence of spontaneously established perpendicular exchange bias in $Co_{49}Pt_{51}$/IrMn bilayers. *J. Appl. Phys.* **2014**, *115*, 17D726. [CrossRef]
39. Shen, J.X.; Kief, M.T. Exchange coupling between NiO and NiFe thin films. *J. Appl. Phys.* **1996**, *79*, 5008–5010. [CrossRef]
40. Hu, J.-G.; Jin, G.-J.; Ma, Y.-Q. Thickness dependence of exchange bias an coercivity in a ferromagnetic layer coupled with and antiferromagnetic layer. *J. Appl. Phys.* **2003**, *94*, 2529. [CrossRef]
41. Zhou, S.M.; Liu, K.; Chien, C.L. Exchange coupling and macroscopic domain structure in a wedged permalloy/FeMn bilayer. *Phys. Rev. B* **1998**, *58*, R14717. [CrossRef]
42. Tang, Y.J.; Roos, B.; Mewes, T.; Demokritov, S.O.; Hillebrands, B.; Wang, Y.J. Enhanced coercivity of exchange-bias Fe/MnPd bilayers. *Appl. Phys. Lett.* **1999**, *75*, 707. [CrossRef]
43. Demarche, J.; Terwagne, G. Precise measurement of the differential cross section from the $^{16}O(\alpha,\alpha)^{16}O$ elastic reaction at 165° and 170° between 2.4 and 6 MeV. *J. Appl. Phys.* **2006**, *100*, 124909. [CrossRef]
44. Gatel, C.; Snoeck, E.; Serin, V.; Fert, A.R. Epitaxial growth and magnetic exchange anisotropy in Fe_3O_4/NiO bilayers grown on MgO(001) and Al_2O_3(0001). *Eur. Phys. J. B* **2005**, *45*, 157–168. [CrossRef]